

Proton decay matrix elements on the lattice

Y. Aoki,^{1,2,*} E. Shintani,^{2,†} and A. Soni^{3,‡}

(RBC and UKQCD collaborations)

¹ *Kobayashi-Maskawa Institute for the Origin of Particles and the Universe (KMI),
Nagoya University, Nagoya 464-8602, Japan*

² *RIKEN-BNL Research Center, Brookhaven National Laboratory, Upton, NY 11973, USA*

³ *High Energy Theory Group, Brookhaven National Laboratory, Upton, NY 11973, USA*

Abstract

Hadronic matrix elements of proton decay are essential ingredients to bridge the grand unification theory to low energy observables like proton lifetime. In this paper we non-perturbatively calculate the matrix elements, relevant for the process of a nucleon decaying into a pseudoscalar meson and an anti-lepton through generic baryon number violating four-fermi operators. Lattice QCD with 2+1 flavor dynamical domain-wall fermions with the *direct* method, which is direct measurement of matrix element from three-point function without chiral perturbation theory, are used for this study to have good control over the lattice discretization error, operator renormalization, and chiral extrapolation. The relevant form factors for possible transition process from an initial proton or neutron to a final pion or kaon induced by all types of three quark operators are obtained through three-point functions of (nucleon)-(three-quark operator)-(meson) with physical kinematics. In this study all the relevant systematic uncertainties of the form factors are taken into account for the first time, and the total error is found to be the range 30%–40% for π and 20%–40% for K final states.

PACS numbers: 11.15.Ha,12.38.Gc,12.10.Dm

*Electronic address: yaoki@kmi.nagoya-u.ac.jp

†Electronic address: shintani@riken.jp

‡Electronic address: adlersoni@gmail.com

I. INTRODUCTION

Proton decay is a smoking gun evidence of physics beyond the standard model and is a natural outcome of Grand Unified Theories (GUTs) [1, 2]. The process occurs through baryon number changing interactions mediated by the heavy new particles. Dominant modes are of X and Y gauge boson exchange for non supersymmetric (SUSY) GUTs and of color-triplet Higgs multiplet for SUSY GUTs [3, 4]. Recent SuperKamiokande experiments report the bound on proton partial lifetime, for instance, $\tau > 8.2 \times 10^{33}$ year for the $p \rightarrow e^+ \pi^0$ channel [5, 6], which is typical for gauge boson exchange, or $\tau > 2.3 \times 10^{33}$ for $p \rightarrow K^+ \bar{\nu}$ [7] and $\tau > 1.6 \times 10^{33}$ for $p \rightarrow K^0 \bar{\mu}^+$ [8], both of which are favored for some SUSY GUTs. There have been many arguments of a constraint on proton lifetime from various types of GUT model so far (see a comprehensive review [9] and reference therein). In order to constrain the parameter space in GUT models with a reliable bound, a removal of every theoretical uncertainty is highly desirable. One of the important elements, which can be made less uncertain from the current knowledge, is the hadronic contribution to proton decay matrix elements. Lattice QCD calculation can lead to reducing the uncertainties in hadronic matrix element of a nucleon decaying into a pseudoscalar meson, and thus it can provide relevant information for the proton lifetime bound and help experimental plans for the future [10].

The estimate of proton decay matrix elements in lattice QCD has been significantly improved by removing systematic errors, one by one, since the first attempts in 1980s [11–13]. A decade ago using Wilson fermion action with quenched QCD, JLQCD collaboration [14] performed an extensive calculation of proton decay matrix elements with both the “*direct*” method, which is a direct measurement of matrix element from three-point functions, and the “*indirect*” method, which is an effective estimate through low-energy constants in tree-level chiral perturbation theory, calculated with two-point functions. Few years later JLQCD and CP-PACS joint collaboration carried out a continuum extrapolation of the low energy constants for the *indirect* analysis [15] to remove the uncertainty due to large discretization error. Within the “*direct*” method, RBC collaboration [16] performed the analysis using domain-wall fermions (DWFs) and a non-perturbative renormalization, where thanks to almost exact chiral symmetry of the DWFs the discretization error of $\mathcal{O}(a)$ is essentially removed and the error of renormalization factor associated with the use of lattice perturbation theory was also eliminated. The RBC collaboration and later RBC/UKQCD

collaborations extended the DWF calculation of the “indirect” method, in which they used the quenched approximation [16] as well as unquenched one containing active two (u and d) and three (adding s) dynamical light flavors [17]. In this way, one of the uncontrolled systematic uncertainty coming from quenched approximation was removed.

A striking, but perhaps not surprising outcome of the comparison of the results from *direct* and *indirect* calculations, though performed only with quenched approximation so far, is that the *indirect* method could overestimate the matrix elements by a factor of about two [16]. Therefore the last step is to perform the *direct* calculation with the three flavor DWF simulation with non-perturbative renormalization of the operators, to remove all the uncontrolled systematic uncertainties in the existing calculations.

In this paper we provide the non-perturbative value of proton decay matrix elements using the *direct* method with the dynamical, $N_f = 2 + 1$ (degenerate u , d and physical s quarks) flavor lattice QCD with DWFs. The DWF ensemble for $N_f = 2 + 1$ at the lattice cutoff $a^{-1} \sim 1.7$ GeV with 300–700 MeV pion masses [18] in RBC/UKQCD collaboration are used for this purpose, and thus this enables us to evaluate hadronic matrix elements including almost all systematic errors on the lattice.

This paper is organized as follows. In section II we explain the definition and property of the matrix elements as well as their relation to the proton partial decay width. The method to extract the matrix elements from three-point function on the lattice is expressed in section III, and in section IV we present our setup and the detailed analysis to obtain the matrix elements and evaluate their systematic uncertainties. Section V is devoted to summary and outlook.

II. PROTON DECAY MATRIX ELEMENT

A. Effective Lagrangian and matrix element

Baryon number violating operators appearing in the leading low-energy effective Hamiltonian are constructed by possible combination of dimension-six (three quarks and one lepton) operators to be $SU(3)$ color singlets and $SU_L(2) \times U_Y(1)$ invariant. Following the notation

of [19–21], four-fermi operators are expressed as

$$O_{abcd}^{(1)} = (D_a^i, U_b^j)_R (q_c^{k\alpha}, l_d^\beta)_L \varepsilon^{ijk} \varepsilon^{\alpha\beta}, \quad (1)$$

$$O_{abcd}^{(2)} = (q_a^{i\alpha}, q_b^{j\beta})_L (U_c^k, l_d)_R \varepsilon^{ijk} \varepsilon^{\alpha\beta}, \quad (2)$$

$$\tilde{O}_{abcd}^{(4)} = (q_a^{i\alpha}, q_b^{j\beta})_L (q_c^{k\gamma}, l_d^\delta)_L \varepsilon^{ijk} \varepsilon^{\alpha\delta} \varepsilon^{\beta\gamma}, \quad (3)$$

$$O_{abcd}^{(5)} = (U_a^i, D_b^j)_R (U_c^k, l_d)_R \varepsilon^{ijk}, \quad (4)$$

with generic lepton field l , and quark field of left-handed part q and right-handed part U and D as up and down type. The indices a, b, c, d denote the generation number of fermion, i, j, k denote color SU(3) indices, and $\alpha, \beta, \gamma, \delta$ are SU(2) indices. The inner product is defined as $(x, y)_{R/L} = x^T C P_{R/L} y$ which has charge conjugation matrix C and chiral projection $P_{R/L}$. The baryon number violation (but preserving $B-L$ number) in GUT models is generally expressed as low-energy effective Hamiltonian with the above six-dimension operators. Leading term of effective Hamiltonian at low energies reads

$$\mathcal{L}^{\mathcal{B}} = \sum_I C^I [(qq)(ql)]^I(\mu) + \dots = - \sum_I C^I [\bar{l}^c \mathcal{O}_{qqq}]^I(\mu) + \dots, \quad (5)$$

where $C^I = C^I(\mu)$ is the Wilson coefficient with renormalization scale μ for each operator i corresponding to Eq.(1)–(4). The details of the (SUSY) GUT is all captured in the coefficients $C^I(\mu)$. Ellipsis means the higher order operators which are suppressed by inverse power of heavy mass scale. The index i within the three-quark operator \mathcal{O}_{qqq} and lepton l in Eq.(5) distinguishes the type of fermion and lepton (flavor and chirality). Three-quark operator is defined as

$$\mathcal{O}_{qqq}^{\Gamma\Gamma'} = (qq)_{\Gamma\Gamma'} = \varepsilon^{ijk} (q^{iT} C P_{\Gamma} q^j) P_{\Gamma'} q^k, \quad (6)$$

with light quark flavor $q = (u, d, s)$, where the color singlet contraction is taken. Dirac spinor indices are omitted in the above equation. In the following we may use simple notations for the three-quark operators as $\mathcal{O}^{\Gamma\Gamma'}$. Γ and Γ' denote the chirality, either R or L and the bracket means the contractions among Dirac spinors.

We calculate the transition matrix elements of the dimension-six operators with an initial nucleon (proton or neutron, $N = p, n$) state and a final state containing a pseudoscalar meson ($P = (\pi, K, \eta)$) and an anti-lepton (\bar{l})

$$\langle P(\vec{p}), l(\vec{q}, s) | [\bar{l}^c \mathcal{O}^{\Gamma\Gamma'}] | N(\vec{k}) \rangle = \bar{v}_l^c(q, s) \langle P(\vec{p}) | \mathcal{O}^{\Gamma\Gamma'} | N(\vec{k}, s) \rangle, \quad (7)$$

including three-dimensional momenta, \vec{p} for final pseudoscalar, \vec{k} for initial nucleon and $\vec{q} = \vec{p} - \vec{k}$ for final lepton which is determined from momentum conservation. Neglecting the electroweak interaction of the lepton, the amplitude $\langle l(\vec{q}, s) | \bar{l}^c | 0 \rangle = \bar{v}_l^c(\vec{q}, s)$ of the lepton part can be captured in the wave function of on-shell lepton state at momentum \vec{q} for spin s component. Furthermore the matrix element in the quark sector can be divided into relevant form factor $W_0(q^2)$ and irrelevant one $W_1(q^2)$ as

$$\langle P(\vec{p}) | \mathcal{O}^{\Gamma\Gamma'} | N(\vec{k}, s) \rangle = P_{\Gamma'} \left[W_0^{\Gamma\Gamma'}(q^2) - \frac{i\not{q}}{m_N} W_1^{\Gamma\Gamma'}(q^2) \right] u_N(k, s). \quad (8)$$

where W_0 and W_1 are defined for each matrix element with the three-quark operator renormalized in \overline{MS} NDR at scale μ , and are functions of square of four momentum transfer $q = k - p$. Using on-shell condition, the total matrix element as shown in Eq.(7) is given by

$$\begin{aligned} \bar{v}_l^c(q, s) \langle P(\vec{p}) | \mathcal{O}^{\Gamma\Gamma'} | N(\vec{k}, s) \rangle &= \bar{v}_l^c(q, s) P_{\Gamma'} \left[W_0^{\Gamma\Gamma'}(q^2) - \frac{i\not{q}}{m_N} W_1^{\Gamma\Gamma'}(q^2) \right] u_N(k, s) \\ &= \bar{v}_l^c(\vec{q}, s) P_{\Gamma'} u_N(\vec{k}, s) W_0^{\Gamma\Gamma'}(0) + O(m_l/m_N), \end{aligned} \quad (9)$$

with $i\not{q}v_l = m_l v_l$ and $W_1 \simeq W_0$ [16]. Since $-q^2 = m_l^2$ is much smaller than nucleon mass squared in the case of $l = e, \nu$, we set $q^2 = 0$ and ignore the second term in Eq.(9). Taking only the relevant form factor will be a good approximation even for $l = \mu$, as $m_\mu/m_N \sim 10\%$ is smaller than the total error of W_0 in this study.

Once we obtain the relevant form factor W_0 in lattice QCD, the partial decay width of the decay $N \rightarrow P + \bar{l}$ is given by

$$\Gamma(N \rightarrow P + \bar{l}) = \frac{m_N}{32\pi} \left[1 - \left(\frac{m_P}{m_N} \right)^2 \right]^2 \left| \sum_I C^I W_0^I(N \rightarrow P) \right|^2 \quad (10)$$

with the perturbative estimate of Wilson coefficient C^I in the GUT models [9]. Note that renormalization scale dependence of C_i and W_0^i cancels out in their multiplication.

We can reduce the number of types of matrix element by using Parity symmetry and isospin symmetry. The different chirality combinations of the matrix elements are related through the Parity transformation as

$$\langle P; \vec{p} | \mathcal{O}^{RL} | N; \vec{k}, s \rangle = \gamma_0 \langle P; -\vec{p} | \mathcal{O}^{LR} | N; -\vec{k}, s \rangle, \quad (11)$$

$$\langle P; \vec{p} | \mathcal{O}^{LL} | N; \vec{k}, s \rangle = \gamma_0 \langle P; -\vec{p} | \mathcal{O}^{RR} | N; -\vec{k}, s \rangle, \quad (12)$$

which indicates that four chirality combinations $(\Gamma\Gamma') = (RL), (LL), (RL), (RR)$ are reduced to two different combinations, $(\Gamma\Gamma') = (RL), (LL)$. In this paper Γ' is fixed in a left-handed

chirality, and thus we define $W_{0,1}^{\Gamma L} \equiv W_{0,1}^{\Gamma}$. Under exchange-symmetry between u and d there is the relation between their isospin partners n and p ,

$$\langle \pi^0 | (ud)_{\Gamma} u_L | p \rangle = \langle \pi^0 | (du)_{\Gamma} d_L | n \rangle, \quad (13)$$

$$\langle \pi^+ | (ud)_{\Gamma} d_L | p \rangle = -\langle \pi^- | (du)_{\Gamma} u_L | n \rangle, \quad (14)$$

$$\langle K^0 | (us)_{\Gamma} u_L | p \rangle = -\langle K^+ | (ds)_{\Gamma} d_L | n \rangle, \quad (15)$$

$$\langle K^+ | (us)_{\Gamma} d_L | p \rangle = -\langle K^0 | (ds)_{\Gamma} u_L | n \rangle, \quad (16)$$

$$\langle K^+ | (ud)_{\Gamma} s_L | p \rangle = -\langle K^0 | (du)_{\Gamma} s_L | n \rangle, \quad (17)$$

$$\langle K^+ | (ds)_{\Gamma} u_L | p \rangle = -\langle K^0 | (us)_{\Gamma} d_L | n \rangle, \quad (18)$$

$$\langle \eta | (ud)_{\Gamma} u_L | p \rangle = -\langle \eta | (du)_{\Gamma} d_L | n \rangle, \quad (19)$$

involving negative sign coming from u and d exchange of interpolation operator of proton and of neutral pion. Furthermore in the SU(2) isospin limit there is an additional relation between Eq.(13) and Eq.(14):

$$\langle \pi^0 | (ud)_{\Gamma} u_L | p \rangle = \sqrt{2} \langle \pi^+ | (ud)_{\Gamma} d_L | p \rangle. \quad (20)$$

Therefore there are twelve principal matrix elements we calculate in this paper.

III. CALCULATION SCHEME FOR THE FORM FACTORS

To obtain the matrix element we make use of the ratio of three-point function of (nucleon)-($O^{\Gamma L}$)-(meson) and two-point function of nucleon and meson. Such a ratio is represented as

$$\begin{aligned} & R_3(t, t_1, t_0; \vec{p}, \mathcal{P}) \\ &= \frac{\sum_{\vec{x}, \vec{x}_1} e^{i\vec{p}(\vec{x}_1 - \vec{x})} \text{tr} [\mathcal{P} \langle 0 | J_P^{\text{gs}}(\vec{x}_1, t_1) \mathcal{O}^{\Gamma L}(\vec{x}, t) \bar{J}_p^{\text{gs}}(\vec{0}, t_0) | 0 \rangle]}{\sum_{\vec{x}, \vec{x}_1} e^{i\vec{p}(\vec{x}_1 - \vec{x})} \langle 0 | J_P^{\text{gs}}(\vec{x}_1, t_1) J_P^{\text{gs}\dagger}(\vec{x}, t) | 0 \rangle \sum_{\vec{x}} \text{tr} [P_4 \langle 0 | J_p^{\text{gs}}(\vec{x}, t) \bar{J}_p^{\text{gs}}(\vec{0}, t_0) | 0 \rangle]} \sqrt{Z_P^{\text{gs}}(\vec{p}) Z_p^{\text{gs}} L_\sigma^3}, \end{aligned} \quad (21)$$

with interpolating field for pseudoscalar J_P and nucleon J_p . Here we introduce the spatial momentum $\vec{p} = 2\pi\vec{n}/L_\sigma$, \vec{n} is integer vector taking from 0 to $L_\sigma - 1$, L_σ is the spatial extension of the lattice. Superposition “gs” of interpolating operator denotes the type of source/sink function is gauge-invariant Gaussian smearing [22]. “tr” represents trace over spinor indices, and \mathcal{P} is a spin projection matrix. In order to obtain the three-point

function in numerator including three-quark operator defined in Eq.(6), we construct quark propagator with sequential source method.

In this calculation we use $\vec{n} = (1, 0, 0), (1, 1, 0)$ for meson momentum and zero nucleon momentum in three-point function. $Z_{P,p}$ indicates the amplitude of overlap of the interpolating field to on-shell state,

$$\langle P(\vec{p}) | J_P^{\text{gs}\dagger}(0) | 0 \rangle = \sqrt{Z_P^{\text{gs}}(\vec{p})}, \quad (22)$$

$$\langle 0 | J_p^{\text{gs}}(0) | p(\vec{0}, s) \rangle = \sqrt{Z_p^{\text{gs}}} u_p(m_N, s), \quad (23)$$

with Dirac spinor normalized by $\bar{u}_p(k, s) u_p(k, s') = 2m_N \delta_{ss'}$ being the momentum of the nucleon $k = (0, 0, 0, im_N)$ and meson $p = (\vec{p}, iE_P)$. Note that the operator of nucleon interpolating field is not uniquely determined, and actually we see that two possible proton operators formed as

$$J_p = \varepsilon^{ijk} (u^{iT} C \gamma_5 d^j) u^k, \quad \varepsilon^{ijk} (u^{iT} C \gamma_4 \gamma_5 d^j) u^k. \quad (24)$$

Since there is equivalence between proton and neutron matrix element as shown in Eq.(13)–(19), we focus on proton case. Numerical comparison between the above two types of nucleon interpolating operator will be shown in the next section.

Taking an enough large time separation of meson-operator ($t_1 - t$) and operator-nucleon ($t - t_0$) in order to suppress the other excited state contamination than an asymptotic state of pseudoscalar and nucleon, the ratio leads to

$$\lim_{t_1-t, t-t_0 \rightarrow \infty} R_3(t, t_1, t_0; p, \mathcal{P}) = R_3^{\text{asym}}(p, \mathcal{P}) = \text{tr} \left[\mathcal{P} P_L (W_0^\Gamma(q^2) - \frac{i \not{q}}{m_N} W_1^\Gamma(q^2)) \right], \quad (25)$$

where q^2 is the squared momentum transfer from the initial proton to the final pseudoscalar meson state $q^2 = (k - p)^2$. We employ two different projection matrices $\mathcal{P} = P_4$ or $iP_4 \gamma_j$ with $P_4 = (1 + \gamma_4)/2$ by which we subtract parity-partner contamination (excited state) to extract form factor from three point function by solving linear equation of

$$R_3^{\text{asym}}(p, P_4) = W_0^\Gamma(q^2) - \frac{i q_4}{m_N} W_1^\Gamma(q^2), \quad (26)$$

$$R_3^{\text{asym}}(p, iP_4 \gamma_j) = \frac{q_j}{m_N} W_1^\Gamma(q^2), \quad (27)$$

and thus W_0 and W_1 can be simultaneously obtained. Hereafter we concentrate on the relevant form factor W_0 .

IV. NUMERICAL CALCULATION OF THE PROTON DECAY FORM FACTORS

A. Lattice setup

We use gauge configurations with dynamical domain-wall fermions of $2 + 1$ flavor at Iwasaki gauge action in lattice size $24^3 \times 64$ at $\beta = 2.13$ which corresponds to $a^{-1} = 1.73(3)$ [18]. This is the same ensemble as previous *indirect* method study [17]. Boundary condition is periodic for gauge field, and spatially periodic and temporally anti-periodic for fermion field. We use four different unitary u , d quark masses in chiral extrapolation, and one unitary and one partially quenched strange-quark mass in the study of strange quark mass dependence for final $K^{0,+}$ kaon state. Explicit chiral symmetry breaking due to finite fifth dimensional lattice as $L_s = 16$ is small in this ensemble [18] (residual mass is $m_{\text{res}} \simeq 3 \times 10^{-3}$), and indeed we take into account residual mass-shift in the chiral extrapolation. For later convenience let us introduce the quark mass \tilde{m} which includes the additive renormalization due to the inexact chiral symmetry of the domain-wall fermions at a finite extension of the fifth dimension. We define

$$\tilde{m} = m + m_{\text{res}}, \quad (28)$$

as the multiplicatively renormalizable mass with m in the lattice action, where residual mass m_{res} for the lattice used in this study has been calculated as $m_{\text{res}} = 0.003152(43)$ [18]. For the nucleon to pion matrix elements we have two controlling variables: \tilde{m}_{ud} for the degenerate u and d quark mass and the squared momentum transfer q^2 . For the nucleon to kaon matrix elements the strange quark mass \tilde{m}_s is an added controlling variable.

When computing two-point and three-point function on the lattice, we employ parameters of gauge-invariant Gaussian smearing with its parameter $(n_G, \sigma) = (40, 5.0)$ for baryon source/sink and $(n_G, \sigma) = (16, 3.0)$ for meson sink including APE smeared link gauge in which we use the parameter $(N, c) = (12, 0.4)$ as defined in [23]. Nucleon source-point t_0 and pseudoscalar sink-point t_1 for three-point function are set to be fixed as $t_0 = 5$ or 37 and $t_1 = 27$ or 59 , and operator in three-point function constructed by sequential source for meson sink moves its position t between t_0 and t_1 with spacial momentum $\vec{p} = (\pi/12, 0, 0), (\pi/12, \pi/12, 0)$. The detailed number of gauge ensembles and source positions employed here are shown in table I. For measurement at $m_{ud}^{\text{sea}} = 0.005$ ensemble we add the statistics in different source and sink points in the same configurations separated in 40

HMC trajectory skips. At $m_{ud}^{\text{sea}} = 0.02, 0.03$ the skipped HMC trajectory in the same source and sink point is 40 and in every source-sink combinations we separated 20 HMC trajectory in order to reduce the autocorrelation effect. At $m_{ud}^{\text{sea}} = 0.01$ the skipped HMC trajectory is 80 and separated trajectory for every source and sink combinations is 40. Note that at the lightest quark mass ($m_{ud}^{\text{sea}} = 0.005$) to increase statistics we further take average over two different source time slices, $t_0 = 5$ and 37, for each gauge configurations (therefore the number of measurements is double of configurations).

The multiplicative renormalization factors to convert the lattice three-quark operators in Eq.(13)–(19) into those in \overline{MS} NDR scheme has been calculated through the RI/MOM non-perturbative renormalization [17] as

$$U(\mu = 2\text{GeV})_{LL} = 0.662(10)(53), \quad (29)$$

$$U(\mu = 2\text{GeV})_{RL} = 0.665(8)(53). \quad (30)$$

The first error is statistical one and the second is systematic one (8% systematic error is estimated in [17] as a truncation effect of perturbative expansion).

In Figure 1 we show the effective mass plot of nucleon, pion and kaon two-point function which consists of denominator of Eq.(21). This is constructed with data at t and $t + 1$, and we can observe the plateau region whose starting point is $t = 5$ for nucleon and $t = 6$ for pseudoscalar. It turns out that the asymptotic state of nucleon and meson state of three point function in Eq.(21) will be reached in the region $t - t_0 \geq 5$ and $t_1 - t \leq 6$ for temporal position of operator t .

B. Measurement of form factor and kinematics

Figures 2 and 3 show the form factor W_0 of the $p \rightarrow \pi^0$ channel obtained by using the asymptotic structure Eqs. (26) and (27) as a function of the time position t of the three-quark operator for each quark masses and momenta. The open and filled symbols correspond to results in two different nucleon interpolating operators, $(q^T C \gamma_5 q)q$ and $(q^T C \gamma_4 \gamma_5 q)q$ respectively. To obtain the value of W_0 , a simultaneous fit of these two effective W_0 is performed at the plateau in the range $13 \leq t \leq 20$, where the two W_0 appear to be consistent and the contamination from the excited states dies out. The same range is used for all the parameters and all the matrix elements. Figures 4 and 5 show $W_0^{R/L}$ for each channel as a function

TABLE I: Lattice parameters used in this paper. Fitting range of pion and Kaon mass is $6 \leq t \leq 23$, and nucleon mass is $5 \leq t \leq 13$. Lattice spacing is $a^{-1} = 1.733$ GeV, which is same value as [18]. Two columns of $-q^2$ are values of squared momentum transfer for each quark masses and two different spatial momentum squared, $|\vec{p}|^2 = (\pi/12)^2, 2(\pi/12)^2$ respectively.

$(m_{ud}^{\text{sea}}, m_s^{\text{sea}})$	$(m_{ud}^{\text{val}}, m_s^{\text{val}})$	m_π	m_K	m_N	$-q^2(\text{GeV}^2)$	# configs.	# meas.	
(0.005,0.04)	(0.005,N/A)	0.1897(5)	N/A	0.656(16)	-0.129	0.241	202	404
	(0.005,0.0343)	N/A	0.3131(5)	N/A	0.017	0.325		
	(0.005,0.04)	N/A	0.3322(5)	N/A	0.039	0.337		
(0.01,0.04)	(0.01,N/A)	0.2420(6)	N/A	0.705(16)	-0.162	0.194	150	150
	(0.01,0.0343)	N/A	0.3328(6)	N/A	-0.035	0.280		
	(0.01,0.04)	N/A	0.3510(6)	N/A	-0.011	0.295		
(0.02,0.04)	(0.02,N/A)	0.3228(6)	N/A	0.790(10)	-0.218	0.137	100	100
	(0.02,0.0343)	N/A	0.3681(6)	N/A	-0.142	0.189		
	(0.02,0.04)	N/A	0.3849(6)	N/A	-0.114	0.208		
(0.03,0.04)	(0.03,N/A)	0.3880(7)	N/A	0.912(11)	-0.391	-0.020	90	90
	(0.03,0.0343)	N/A	0.4003(6)	N/A	-0.364	-0.000		
	(0.03,0.04)	N/A	0.4160(6)	N/A	-0.330	0.025		

of q^2 obtained by the above fitting.

The form factors in the physical kinematics are calculated from the extrapolation or interpolation with momentum and quark mass. For the physical kinematics of proton decay into meson and lepton final state, $-q^2$ is equivalent to lepton mass squared in the relevant form factor $W_0(q^2)$. In the lattice computation, however, the quark masses are other parameters that need to be tuned toward the physical pion and kaon masses. Therefore we have all together three parameters to tune: degenerate u, d quark mass \tilde{m}_{ud} , strange quark mass \tilde{m}_s and meson momentum $|\vec{p}|$. In our simulation, the $\tilde{m}_{ud} \rightarrow \tilde{m}_{ud}^{\text{phys}}$ limit is taken by an extrapolation, $\tilde{m}_s \rightarrow \tilde{m}_s^{\text{phys}}$ limit is taken by an interpolation, where physical quark mass is realized by the limit,

$$\tilde{m}_{ud} \rightarrow \tilde{m}_{ud}^{\text{phys}} = 0.001385, \quad (31)$$

$$\tilde{m}_s \rightarrow \tilde{m}_s^{\text{phys}} = 0.03785, \quad (32)$$

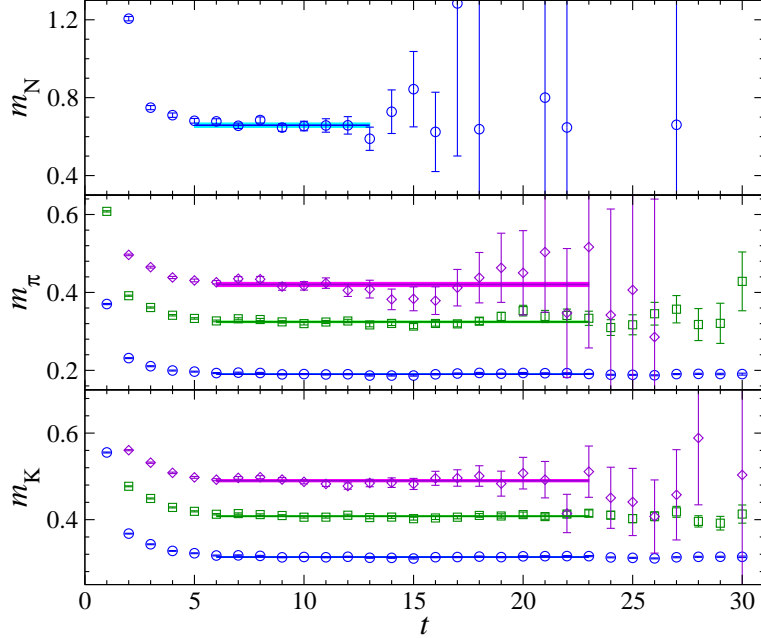


FIG. 1: Effective mass plot of nucleon (top), pion (middle) and Kaon (bottom) at momentum square $n_p^2 = 0$ (circle), $n_p^2 = 1$ (square), $n_p^2 = 2$ (diamond) which correspond to $\vec{p} = (0, 0, 0), (\pi/12, 0, 0), (\pi/12, \pi/12, 0)$ respectively. For nucleon we use gauge-invariant Gaussian source/sink, and for meson we use (Kuramashi-)wall source and gauge-invariant Gaussian sink. This is for the lightest quark mass $m_{ud} = 0.005$ and $m_s = 0.0343$. Solid line (colored band) indicate the central value (statistical error) obtained by fitting.

with the values to reproduce the experimental hadron mass ratios, m_π/m_Ω and m_K/m_Ω , the pion and kaon mass over the mass of Ω^- [18].

We employ two different procedures for taking the above limit. One is to use the global fit with a function that depends on both quark mass and q^2 , and thus W_0 at physical point is straightforwardly obtained. The other is to sequentially take both limits; first $q^2 \rightarrow 0$ and then take the quark mass to the physical point. In this procedure W_0 at physical point is obtained by the second limit. In the next section we will show numerical results with these procedures.

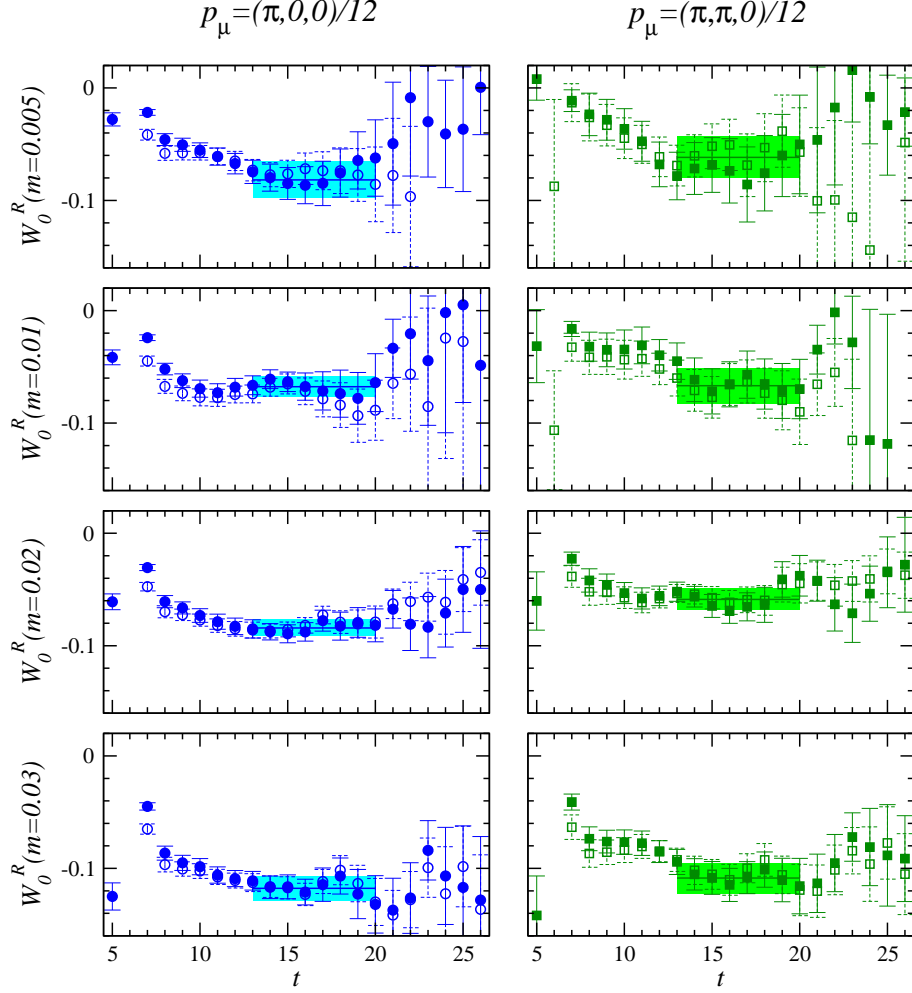


FIG. 2: W_0^R for $p \rightarrow \pi^0$ decay channel is plotted as a function of operator time (t in Eq. (21)). The proton source is located at $t = 5$, and the π^0 sink is at $t = 27$. Different symbols show the two different proton interpolating fields, which correspond to $(u^T C \gamma_5 d)u$ (open) and $(u^T C \gamma_4 \gamma_5 d)u$ (filled). The horizontal solid line indicates the central value of constant fit to the both plateaus in the range $13 \leq t \leq 20$ simultaneously. The shaded area indicates 1-sigma error bound.

C. Extrapolation to physical kinematics with global fitting

The global fitting to obtain the form factor in the physical kinematics uses

$$F_{W_0}^{\pi,\eta}(\tilde{m}_{ud}, q^2) = A_0 + A_1 \tilde{m}_{ud} + A_2 q^2, \quad (33)$$

$$F_{W_0}^K(\tilde{m}_{ud}, \tilde{m}_s, q^2) = B_0 + B_1 \tilde{m}_{ud} + B_2 \tilde{m}_s + B_3 q^2, \quad (34)$$

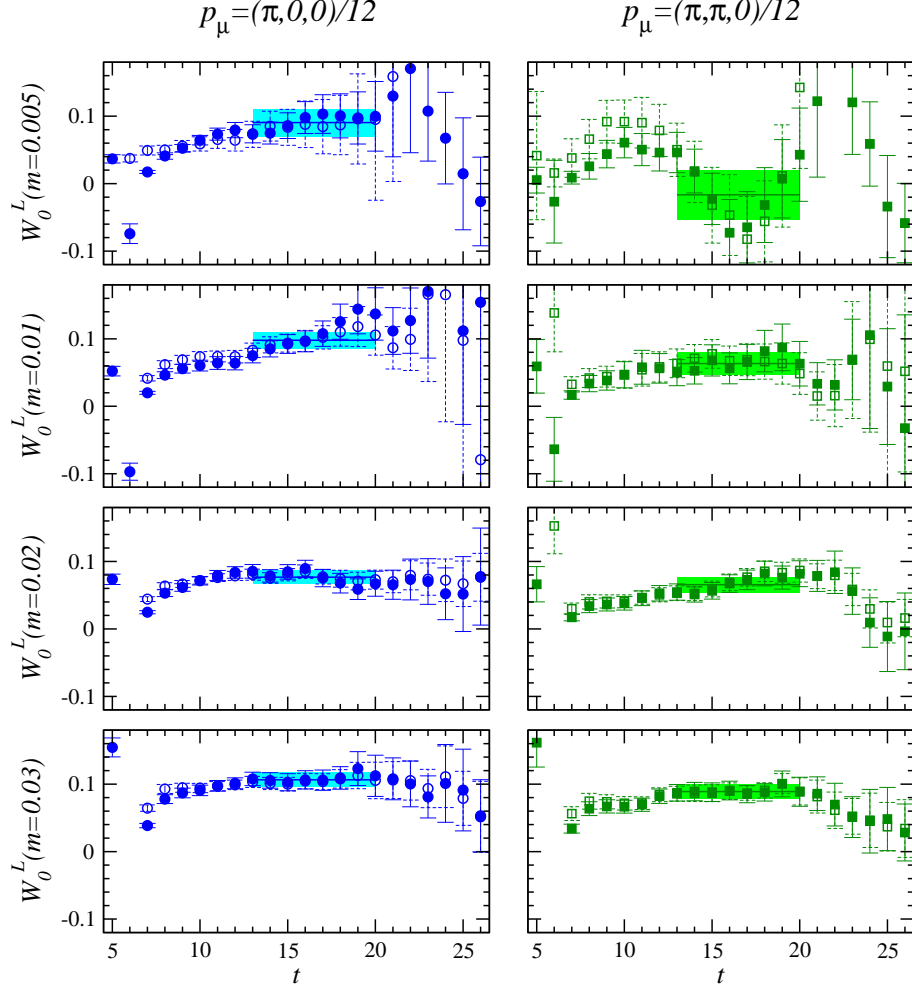


FIG. 3: W_0^L for $p \rightarrow \pi^0$ decay channel is plotted as a function of operator time. Symbols are same as in Figure 2.

with free parameters A_i and B_i . $F_{W_0}^{\pi,\eta}$ is used for the pion or η final state, $F_{W_0}^K$ for the kaon final state. This procedure is the same as that employed in the previous study [16]. We use four different quark masses, two different strange quark masses and the two lowest non-zero spacial momenta, and therefore the total number of data points is eight for π and η or sixteen for the kaon final states. The results obtained with the global fit using all the data are shown in the second column in Table II. It turns out that the simple linear function as described in Eq.(33) and (34) is in good agreement with the lattice data for all channels, which is indicated by the reasonable χ^2/dof (≤ 1.4). The fit results $F_{W_0}^{\pi,\eta}(\tilde{m}_{ud}^{\text{phys}}, q^2)$, $F_{W_0}^K(\tilde{m}_{ud}^{\text{phys}}, \tilde{m}_s^{\text{phys}}, q^2)$ at the physical masses are shown in Figs. 4 and 5.

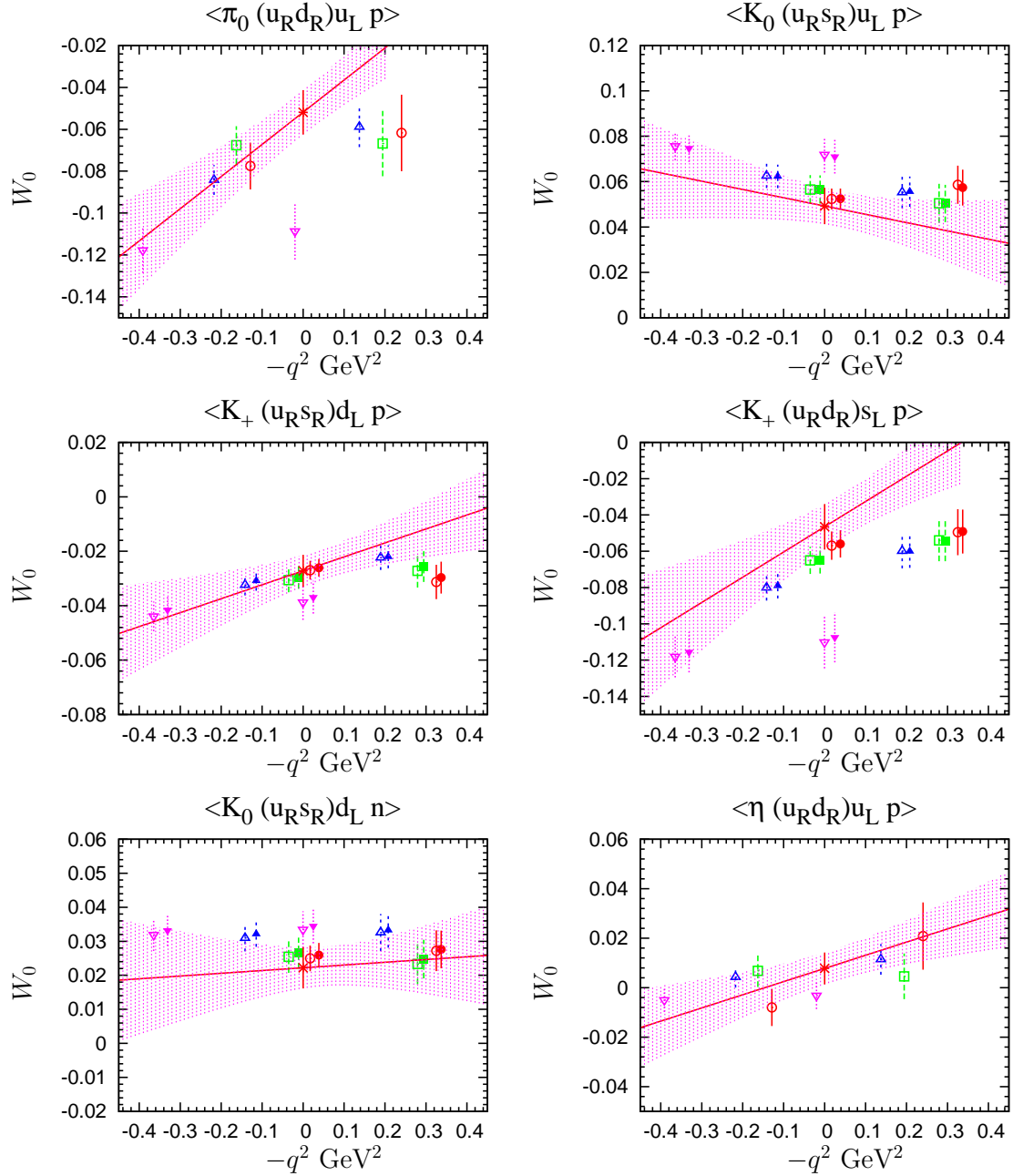


FIG. 4: q^2 dependence of $W_0^R(q^2)$ at all quark masses in the lattice unit. We plot the results at $m_{ud} = 0.005$ (circle), $m_{ud} = 0.01$ (square), $m_{ud} = 0.02$ (upper-triangle) and $m_{ud} = 0.03$ (down-triangle). In the figure for $K^{0,+}$, results at $m_s = 0.0343$ represent open symbol and filled symbol at $m_s = 0.04$. In addition we also show the global fit function in the physical quark mass as solid line and its error band. The star symbol is a result in the physical kinematics using global fit.

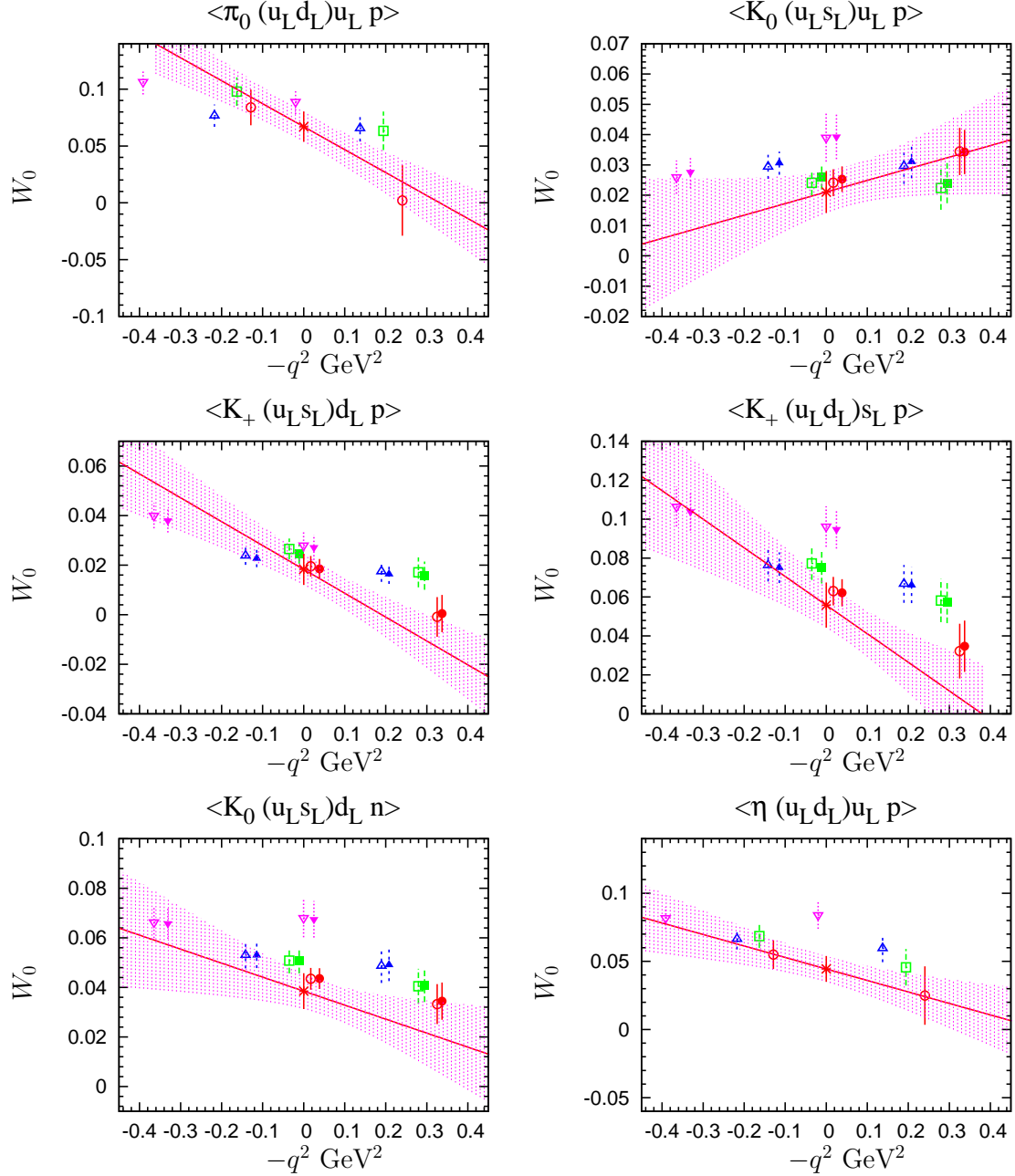


FIG. 5: q^2 dependence of $W_0^L(q^2)$ at all quark masses. Symbols are same as Figure 4.

D. Extrapolation to physical kinematics with sequential fitting

In this procedure we first take the linear extrapolation or interpolation to $q^2 = 0$ with two spatial momentum points in each mass \tilde{m} and second take a chiral extrapolation to physical quark mass. Figure 6 and 7 plot the results at $q^2 = 0$ point as a function of \tilde{m}_{ud} after taking

the $q^2 = 0$ limit. In the chiral extrapolation of the data at $q^2 = 0$ the fitting function is

$$f_{W_0}^{\pi,\eta}(\tilde{m}_{ud}) = a_0 + a_1\tilde{m}_{ud}, \quad (35)$$

$$f_{W_0}^K(\tilde{m}_{ud}, \tilde{m}_s) = b_0 + b_1\tilde{m}_{ud} + b_2\tilde{m}_s, \quad (36)$$

for the pion, η final state or kaon final state respectively. Here a_i and b_i are the free fitting parameters. From Figure 6 and 7 we observe that the linear function well describes the lattice results for each matrix elements in four different mass points. Actually the χ^2/dof for all matrix elements are satisfied with $\chi^2/\text{dof} \lesssim 2$. The results are shown in Table II (see the column marked as ‘‘Sequential’’).

E. Systematic errors

The systematic errors due to unphysical quark mass and kinematics used in the simulation (combined mass and q^2 limit), finite volume and non-zero lattice spacing will be discussed in this section. This work uses the lattice scale estimated in Ref. [18] and the renormalization constant shown in Eq.(29) and Eq.(30). To yield the total error apart from the statistical error of the form factor we add in quadrature the systematic errors in the extrapolation, finite size effect and lattice artifact together with the error of lattice scale and of the non-perturbative renormalization procedure.

At the target mass and momentum point $(\tilde{m}_{ud}, \tilde{m}_s, q^2) = (\tilde{m}_{ud}^{\text{phys}}, \tilde{m}_s^{\text{phys}}, 0)$, no chiral singularity is expected. Therefore, if the simulations are made closer to the target, the linear approximation to the fitting function becomes arbitrary precise. However, as the simulated points might not be close enough to assume the linearity, we need to assess the systematic error due to the choice of this approximation. This systematic error is regarded as the effect of higher order than $O(\tilde{m}_{ud})$ and $O(q^2)$. Note that the higher order effect than $O(\tilde{m}_s)$ is safely neglected as its variation around the physical point is very small as can be estimated by comparing the results with $m_s = 0.0343$ and 0.04 in Figs. 4 and 5.

As the main results of the relevant form factors we employ those by the global fit with $0.005 \leq m_{ud} \leq 0.03$ (see in the second column of Table II). For the convenience of later discussion we define the different fitting ranges as

$$r_{\text{full}} : [0.005, 0.03], \quad r_{\text{heavy}} : [0.01, 0.03], \quad r_{\text{light}} : [0.005, 0.02] \quad (37)$$

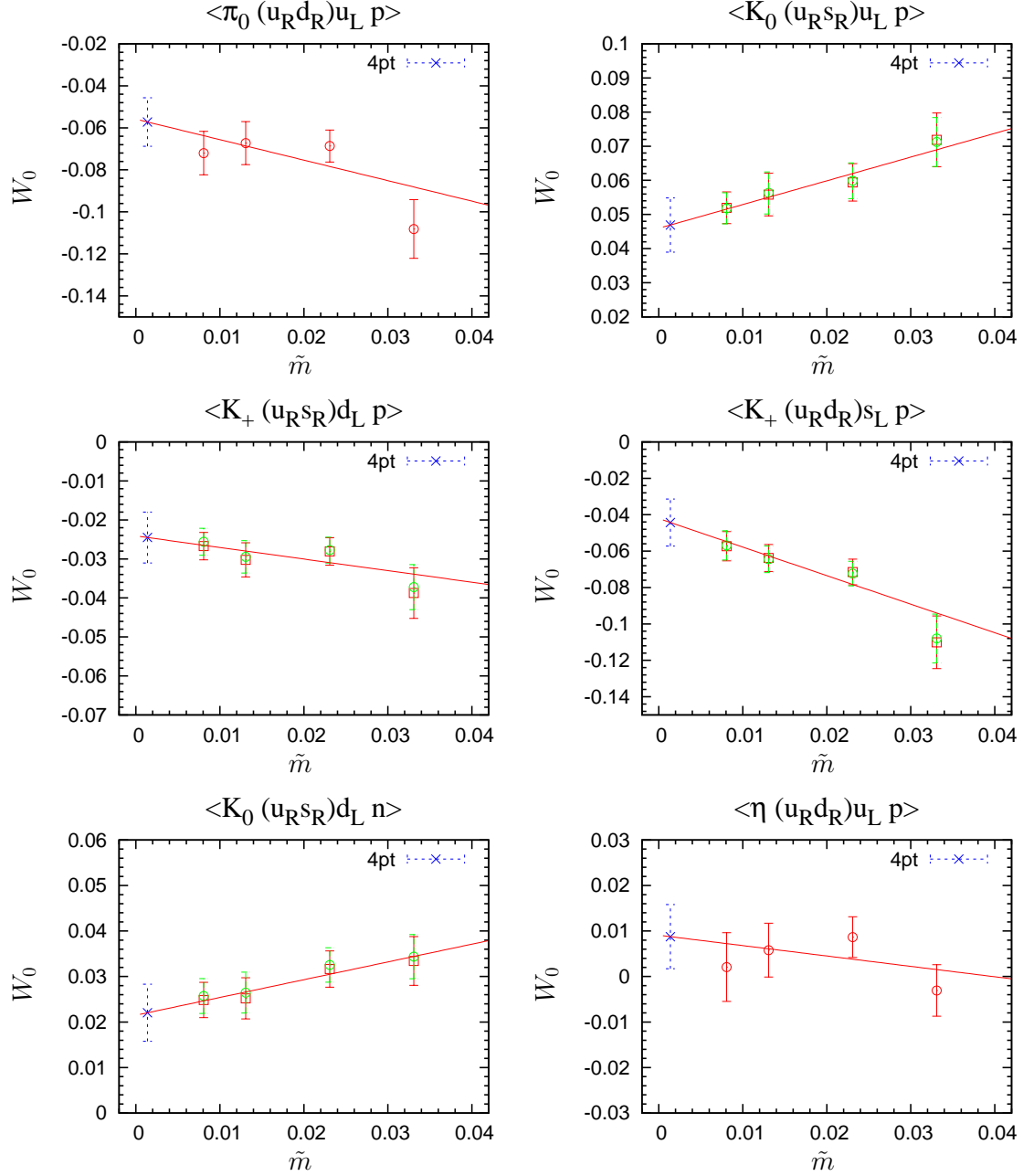


FIG. 6: Results of $W_0^R(0)$ at different $\tilde{m} = m_{ud} + m_{\text{res}}$. The different open symbols shown in the matrix element of Kaon final state are the results at different partially quenched strange quark mass $m_s = 0.0343$ (circle), $m_s = 0.04$ (square). Straight lines show linearly fit function with all four quark masses. For the matrix element of $p \rightarrow K$, these are the results after taking the physical strange quark mass. The cross symbol is result at physical light and strange mass with four fitting points and star symbol is with three fitting points.

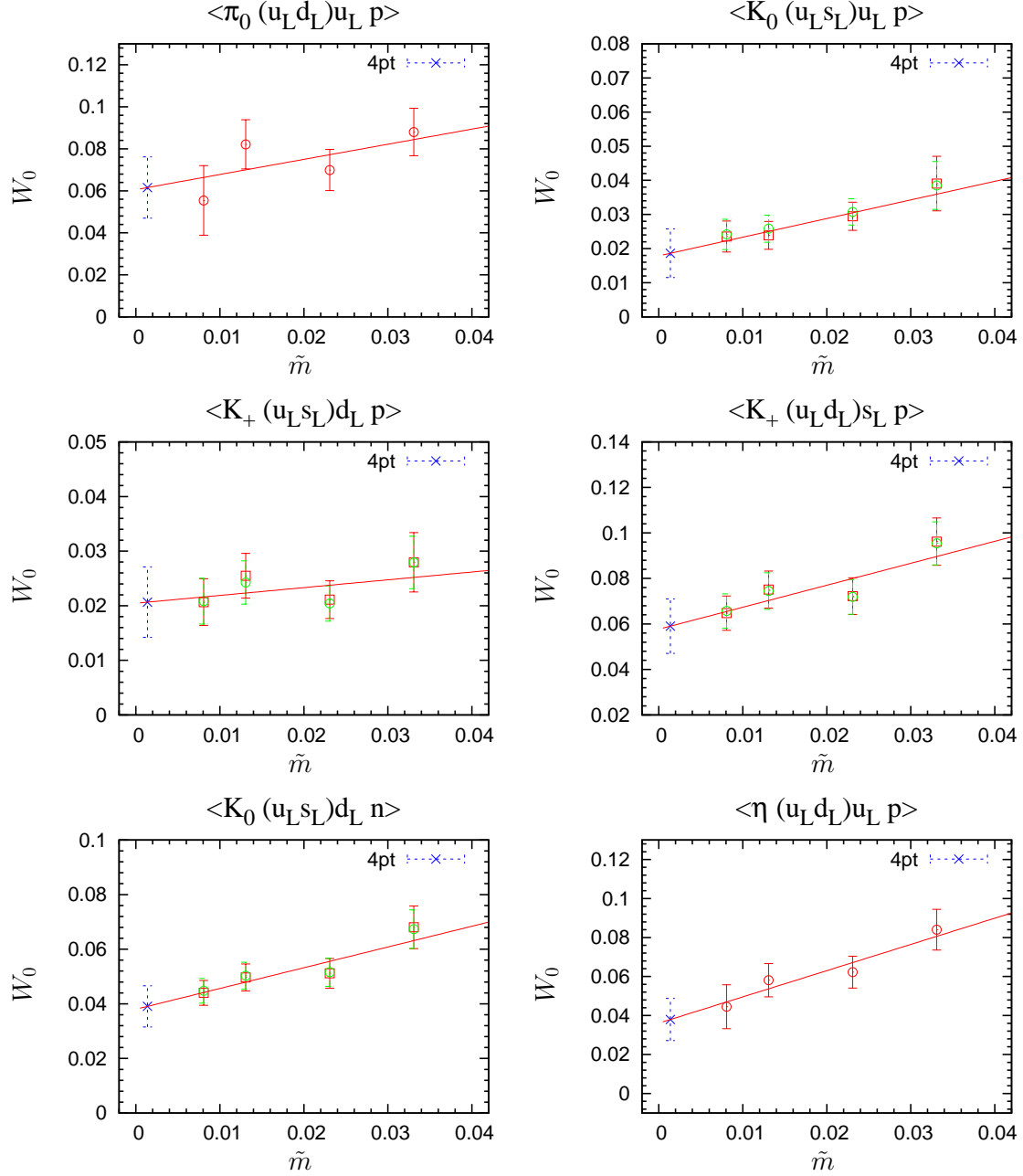


FIG. 7: Results of $W_0^L(0)$ with same symbols as Fig.6.

which are also used in Table II. The variations of results removing the largest \tilde{m}_{ud} from the global fit, removing the smallest \tilde{m}_{ud} from the global fit and the result in sequential fit from the main result provide the systematic errors coming from uncertainty of the fitting function for the extrapolation to the physical kinematics and finite size effect (FSE).

The uncertainty in the extrapolation due to higher order effect than linearity of quark

mass (and also q^2) is estimated by variance between results in r^{full} and r^{light} and variance between results with global fit and sequential fit. By comparing the region with and without heavy mass $m = 0.03$ which is the strange quark mass, we estimate the $O(\tilde{m}^2)$ effect. Furthermore since sequential fitting procedure, explained in the previous subsection, takes into account the mass-dependence of q^2 slope, we estimate the systematic error of the extrapolation to the physical kinematics as a part of the higher order effect, *e.g.* $\mathcal{O}(\tilde{m}q^2)$ terms, beyond the \tilde{m} and q^2 linear approximation by comparing with results in the global fit.

On the other hand the estimate of FSE using variance between results in r^{full} and r^{heavy} expects to probe at least a part of FSE since the lightest point is affected most from the FSE rather than higher order mass effect. Such estimate of FSE has been known in the calculation of the nucleon axial charge g_A [24, 25] in which significant FSE seemed to be observed in the lightest quark mass in the same gauge ensemble. (Furthermore this is also suggested noting that the relevant form factor W_0 for a pion final state is proportional to $1 + g_A$ in the leading order of baryon chiral perturbation theory, see Ref. [16]). Therefore neglecting data at the lightest mass $m = 0.005$ from the fitting region might include less contamination of FSE (see also Fig. 10 of Ref. [25]).

As a consequence the systematic error including both $O(\tilde{m}^2)$, $O((q^2)^2)$, $O(\tilde{m}q^2)$ and FSE is evaluated by the quadrature of variances of (global, sequential) fitting results in the range of r^{full} and maximum variance between global fitting results in the range of $(r^{\text{full}}, r^{\text{light}})$ and $(r^{\text{full}}, r^{\text{heavy}})$ although it might be conservative. The magnitude of the above is shown in the column denoted as “Extrapolation” in Table III.

The discretization error of $O(a)$ may arise from the inexact chiral symmetry due to finite L_s , which is of order $m_{\text{res}} \simeq 3 \times 10^{-3}$ and thus safely neglected. Here the dominant discretization error at $O(a^2)$ has been estimated using the scaling study of hadronic observable performed with this and finer lattice ensembles [18]. The observed discrepancy in the spectroscopy of light meson (Fig. 26 in Ref. [18]) with the two lattice spacings is up to 1–2 %, which amounts to about 5% discretization error for the form factor W_0 assuming the $O(a^2)$ scaling. We take this 5% as the $O(a^2)$ error, whose magnitude appears as the naive estimate using the power counting $(a\Lambda_{\text{QCD}})^2 \sim 0.02$ with $\Lambda_{\text{QCD}} = 250$ MeV.

In addition to all above, we take into account the error coming from uncertainty of lattice spacing which is given in error of $a^{-1} = 1.73(3)$ GeV and the one for the renormalization constant which are given in Eq.(29) and (30).

TABLE II: Table of results for renormalized $W_0^{R/L}(\mu = 2\text{GeV})$ in GeV^2 after global and sequential fitting. The error is only statistical one. For global fitting, we show the results with three different fitting mass-ranges, which are all range $0.005 \leq m_{ud} \leq 0.03$ (r^{full}), exclude the heaviest mass, $m_{ud} = 0.03$, (r^{light}) and exclude the lightest mass, $m_{ud} = 0.005$, (r^{heavy}). For the sequential fitting, we show the results with all mass range.

matrix element	Global				Sequential	
	r^{full}	χ^2/dof	r^{light}	r^{heavy}	r^{full}	χ^2/dof
$\langle \pi^0 (ud)_{RuL} p \rangle$	-0.103(23)	1.4	-0.132(29)	-0.072(34)	-0.114(22)	2.2
$\langle \pi^0 (ud)_{LuL} p \rangle$	0.133(29)	1.4	0.156(41)	0.142(38)	0.123(28)	1.1
$\langle K^0 (us)_{RuL} p \rangle$	0.098(15)	0.4	0.103(19)	0.092(29)	0.093(15)	0.1
$\langle K^0 (us)_{LuL} p \rangle$	0.042(13)	0.4	0.044(16)	0.037(20)	0.037(14)	0.1
$\langle K^+ (us)_{RdL} p \rangle$	-0.054(11)	0.8	-0.060(13)	-0.052(21)	-0.049(13)	0.6
$\langle K^+ (us)_{LdL} p \rangle$	0.036(12)	0.8	0.040(15)	0.041(18)	0.041(12)	0.6
$\langle K^+ (ud)_{RSL} p \rangle$	-0.093(24)	0.6	-0.108(28)	-0.082(39)	-0.088(25)	0.9
$\langle K^+ (ud)_{LSL} p \rangle$	0.111(22)	0.6	0.121(28)	0.115(37)	0.117(23)	0.7
$\langle K^+ (ds)_{RuL} p \rangle$	-0.044(12)	0.1	-0.043(14)	-0.041(20)	-0.044(12)	0.1
$\langle K^+ (ds)_{LuL} p \rangle$	-0.076(14)	0.3	-0.082(17)	-0.076(24)	-0.078(14)	0.5
$\langle \eta (ud)_{RuL} p \rangle$	0.015(14)	1.3	-0.002(19)	0.031(19)	0.017(14)	1.2
$\langle \eta (ud)_{LuL} p \rangle$	0.088(21)	0.7	0.094(29)	0.094(28)	0.076(21)	0.4

We ignore the partially quenched effect of strange quark, which is due to the small mismatch of the sea and valence strange masses, for the matrix element of K meson final state. Since the valence strange quark mass dependence of W_0 is negligibly small as shown in Fig.6 and Fig.7, this effect is also negligible. Note that we also do not consider the effect of disconnected diagrams in the matrix elements of the η in the final state, but note that the result is valid assuming flavor SU(3) degenerate valence quark $m_{ud}^{\text{val}} = m_s^{\text{val}}$ and ignoring partially quenched effect of strange quark.

F. Results of proton decay matrix elements

Table III summarizes the results of the relevant form factor $W_0(q^2)$ of proton decay for all the principal matrix elements Eqs. (13), (15)-(19) at $q^2 = 0$. The central values are those obtained with the global fit on q^2 and the simulated quark masses for the physical kinematics $\tilde{m}_{ud} \rightarrow \tilde{m}_{ud}^{\text{phys}}$, $\tilde{m}_s \rightarrow \tilde{m}_s^{\text{phys}}$ and $q^2 \rightarrow 0$, with the r^{full} range for m_{ud} , which has already been shown in Table II. Values in the first parentheses are the statistical errors. The systematic error budget is shown in the last four columns. These four errors are added in quadrature to give the total systematic error shown in the second parenthesis for each form factor value.

Figure 8 shows the results of the form factors with the error bars expressing the total error of statistical and systematic errors added quadrature, which are marked as “ $N_f = 2 + 1$ ”. The two panels compare the results with old ones using some approximation. The left panel compares against the results with quenched approximation in *direct* method [16]. The right panel shows those with the *indirect* method in the same ensembles [17]. The sizable error for “ $N_f = 2 + 1$ ” in the current analysis prevents us from seeing any visible difference from the quenched or *indirect* results. For phenomenological application, however, one should clearly use the $N_f = 2 + 1$ results with their total error instead of the previous results, because each approximations lead to an unspecified systematic uncertainty.

V. SUMMARY AND OUTLOOK

We have presented the lattice calculation of proton decay matrix elements using $2 + 1$ flavor dynamical domain-wall fermions, essential ingredients to reliably estimate the nucleon lifetime in grand unified theories. The *direct* method using three-point function (nucleon)-(operator)-(meson), with non-perturbative renormalization, was applied on a volume $L_\sigma^3 \simeq 3 \text{ fm}^3$. Previous calculations had unestimated systematic uncertainties on the matrix elements at the physical kinematics. This work made it possible to control these uncertainties for the first time, by removing most of them, while remaining uncertainties were given with their estimates. The uncertainties that have been eliminated are those due to the quenched approximation [16] and the use [17] of the *indirect* method with the tree-level baryon chiral perturbation theory. The estimated uncertainties are the combined errors from chiral extrap-

TABLE III: Final results of renormalized $W_0^{L/R}(\mu = 2\text{GeV})$ for individual matrix elements and error budget of statistical and systematic uncertainties. The first and second errors in $W_0^{L/R}$ represent statistical and systematic ones respectively. The third column denotes total error which is estimated by adding in quadrature statistical and systematic errors. The fourth column denoted as χ shows the systematic error of mass and momentum extrapolation/interpolation estimated by the variance of extrapolation to physical kinematics and fifth column is uncertainties from lattice artifacts explained in the text. The last two columns show the uncertainties of renormalization factor (ΔZ) and lattice spacing (Δa^{-1}). We also show the $p \rightarrow \pi^+\bar{\nu}$ decay matrix element using SU(2) isospin relation in Eq.(20).

Matrix element	$W_0(\mu = 2\text{GeV})$	GeV ²	Total error Systematic error budget				
			(%)	χ	$\mathcal{O}(a^2)$	ΔZ	Δa^{-1}
$\langle \pi^0 (ud)_{RuL} p \rangle$	-0.103 (23)	(34)	40	0.033	0.005	0.008	0.004
$\langle \pi^0 (ud)_{LuL} p \rangle$	0.133 (29)	(28)	30	0.026	0.007	0.011	0.005
$\langle \pi^+ (ud)_{RdL} p \rangle$	-0.146 (33)	(48)	40	0.047	0.007	0.011	0.006
$\langle \pi^+ (ud)_{LdL} p \rangle$	0.188 (41)	(40)	30	0.037	0.010	0.016	0.007
$\langle K^0 (us)_{RuL} p \rangle$	0.098 (15)	(12)	20	0.007	0.005	0.008	0.003
$\langle K^0 (us)_{LuL} p \rangle$	0.042 (13)	(8)	36	0.007	0.002	0.003	0.001
$\langle K^+ (us)_{RdL} p \rangle$	-0.054 (11)	(9)	26	0.008	0.003	0.004	0.002
$\langle K^+ (us)_{LdL} p \rangle$	0.036 (12)	(7)	39	0.007	0.002	0.003	0.001
$\langle K^+ (ud)_{RsL} p \rangle$	-0.093 (24)	(18)	32	0.016	0.005	0.008	0.003
$\langle K^+ (ud)_{LsL} p \rangle$	0.111 (22)	(16)	25	0.012	0.006	0.009	0.004
$\langle K^+ (ds)_{RuL} p \rangle$	-0.044 (12)	(5)	30	0.003	0.002	0.004	0.002
$\langle K^+ (ds)_{LuL} p \rangle$	-0.076 (14)	(9)	22	0.006	0.004	0.006	0.003
$\langle \eta (ud)_{RuL} p \rangle$	0.015 (14)	(17)	147	0.017	0.001	0.001	0.001
$\langle \eta (ud)_{LuL} p \rangle$	0.088 (21)	(16)	30	0.014	0.004	0.007	0.003

olation and finite volume, discretization error, error in the non-perturbative renormalization and the estimate of the lattice scale. The relevant form factors $W_0(q^2 = 0)$ of the twelve principal matrix elements Eqs. (13), (15)-(19), from which one can calculate those for all the nucleon to pseudoscalar meson process, has been evaluated and summarized in Table III

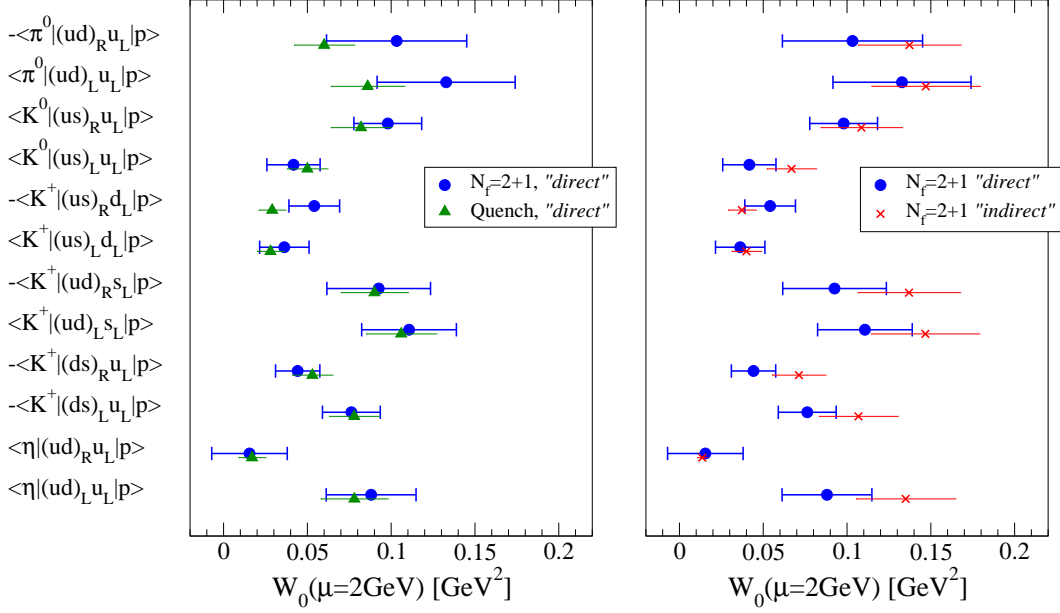


FIG. 8: Summary of $W_0^{L/R}(\mu = 2\text{GeV})$ for twelve principal matrix elements. Filled circles show the present results, and for the comparison the results in quenched QCD (open circle) and indirect method using chiral perturbation theory (cross) are plotted in the same row.

with their error estimates.

In this paper we have established an estimate of proton decay matrix element with all the errors and note that the errors are fairly large (30%–40% for π final state and 20%–40% total error for K final state). One of the major uncertainty is the statistical error, especially for $p \rightarrow e^+\pi^0$ decay mode, and that could have influenced the size of the error of combined chiral extrapolation and finite volume effect. A significant improvement of the current results is expected by adopting the newly developed technique for reduction of the statistical error [26], which will be addressed in future work. We want to emphasize, though, for now in any serious phenomenological application one should use the results in this study with their total errors.

Acknowledgments

We thank the members of RBC/UKQCD collaborations for their valuable help with comments and encouragement. We especially would like to thank Peter Boyle, Paul Cooney,

Chris Dawson, Luigi Del Debbio, Taku Izubuchi, Chulwoo Jung, Adam Lichtle, Chris Maynard, Robert Tweedie. Numerical calculations were performed on QCDOC computers of USQCD collaboration and RIKEN BNL Research Center for which we thank US DOE and RIKEN BNL Research Center. A. S. is supported by U.S. DOE contract DE-AC02-98CH10886. This work is also supported, in part, by JSPS Kakenhi Grant Nos. 21540289, 22224003 (YA), and by MEXT Kakenhi Grant Nos. 23105714 (ES) .

-
- [1] J. C. Pati and A. Salam, Phys. Rev. Lett. **31**, 661 (1973).
 - [2] H. Georgi and S. L. Glashow, Phys. Rev. Lett. **32**, 438 (1974).
 - [3] J. Hisano, H. Murayama, and T. Yanagida, Nucl. Phys. **B402**, 46 (1993), hep-ph/9207279 .
 - [4] H. Murayama and A. Pierce, Phys. Rev. **D65**, 055009 (2002), hep-ph/0108104 .
 - [5] H. Nishino *et al.* (Super-Kamiokande), Phys.Rev.Lett. **102**, 141801 (2009), arXiv:0903.0676 .
 - [6] H. Nishino *et al.* (Super-Kamiokande), Phys.Rev. **D85**, 112001 (2012), arXiv:1203.4030 .
 - [7] K. Kobayashi *et al.* (Super-Kamiokande), Phys. Rev. **D72**, 052007 (2005), hep-ex/0502026 .
 - [8] C. Regis *et al.* (Super-Kamiokande Collaboration), (2012), arXiv:1205.6538 [hep-ex] .
 - [9] P. Nath and P. Fileviez Perez, Phys. Rept. **441**, 191 (2007), arXiv:hep-ph/0601023 .
 - [10] K. Abe, T. Abe, H. Aihara, Y. Fukuda, Y. Hayato, *et al.*, (2011), arXiv:1109.3262 [hep-ex] .
 - [11] Y. Hara, S. Itoh, Y. Iwasaki, and T. Yoshie, Phys. Rev. **D34**, 3399 (1986).
 - [12] K. C. Bowler, D. Daniel, T. D. Kieu, D. G. Richards, and C. J. Scott, Nucl. Phys. **B296**, 431 (1988).
 - [13] M. B. Gavela *et al.*, Nucl. Phys. **B312**, 269 (1989).
 - [14] S. Aoki *et al.* (JLQCD), Phys. Rev. **D62**, 014506 (2000), hep-lat/9911026 .
 - [15] N. Tsutsui *et al.* (CP-PACS), Phys. Rev. **D70**, 111501 (2004), hep-lat/0402026 .
 - [16] Y. Aoki, C. Dawson, J. Noaki, and A. Soni, Phys. Rev. **D75**, 014507 (2007), hep-lat/0607002 .
 - [17] Y. Aoki *et al.* (RBC and UKQCD), Phys. Rev. **D78**, 054505 (2008), arXiv:0806.1031 [hep-lat] .
 - [18] Y. Aoki *et al.* (RBC and UKQCD), Phys.Rev. **D83**, 074508 (2011), arXiv:1011.0892 [hep-lat] .
 - [19] S. Weinberg, Phys. Rev. Lett. **43**, 1566 (1979).

- [20] F. Wilczek and A. Zee, Phys. Rev. Lett. **43**, 1571 (1979).
- [21] L. F. Abbott and M. B. Wise, Phys. Rev. **D22**, 2208 (1980).
- [22] C. Alexandrou, S. Gusken, F. Jegerlehner, K. Schilling, and R. Sommer, Nucl.Phys. **B414**, 815 (1994), arXiv:hep-lat/9211042 [hep-lat] .
- [23] M. Lin *et al.* (RBC and UKQCD), PoS **Lattice 2012**, 172 (2012).
- [24] T. Yamazaki *et al.* (RBC and UKQCD), Phys. Rev. Lett. **100**, 171602 (2008), arXiv:0801.4016 .
- [25] T. Yamazaki *et al.*, Phys. Rev. **D79**, 114505 (2009), arXiv:0904.2039 [hep-lat] .
- [26] T. Blum, T. Izubuchi, and E. Shintani, (2012), arXiv:1208.4349 [hep-lat] .